

Chapter 6

Design of Hovering Orbit and Fuel Consumption Analysis for Spacecraft Considering J_2 Perturbation



Liang Zhang, Tao Song, Hao Ding, and Honghao Liu

Abstract Spacecraft hovering belongs to close range space operations and is mainly applied to on-orbit service of spacecraft. In on-orbit service, the distance between two hovering spacecraft is generally within the range of 0–10 m, whose numerical magnitude is relatively small compared to the orbital radius, so the influence of space perturbation must be considered. In order to improve the accuracy of hovering position, this paper introduces J_2 perturbation into the relative dynamics model of the spacecraft and derives high-precision hovering control equations. Furthermore, the influence of eccentricity and semimajor axis on the hovering control is obtained through an example. Then, using the fuel consumption calculation formula, the distribution of the fuel consumption of the hovering spacecraft is given, when the spacecraft is hovering at different positions in a fixed orbital period. Considering the limited carrying capacity of fuel, the fuel consumption at different hovering positions was analyzed for the same hovering distance, and the problem of determining the hovering position was solved to reduce fuel consumption.

6.1 Introduction

With the continuous advancement of people's exploration of space, it is necessary to extend the lifespan of spacecraft to ensure that they can perform space missions more stably and continuously in unknown space. On-orbit Service (OOS) technology is mainly applied to the maintenance, repair, and upgrade of spacecraft in operation, in order to extend the service life of the spacecraft [1–3]. Spacecraft hovering is a formation configuration with relatively stationary positions, and this fixed state characteristic can provide a stable working environment for on-orbit service, so that spacecraft can successfully complete space operations. Therefore, the control of hovering orbit is the key to achieving the design of spacecraft hovering orbit.

L. Zhang (✉) · T. Song · H. Ding · H. Liu
College of Mechanical and Architectural Engineering, Taishan University, Tai'an 271000,
Shandong, China
e-mail: zhang_liang473@126.com

© The Author(s), under exclusive license to Springer Nature Singapore Pte Ltd. 2024
R. Kountchev et al. (eds.), *Proceedings of International Conference on Artificial Intelligence and Communication Technologies (ICAICT 2023)*, Smart Innovation, Systems and Technologies 368, https://doi.org/10.1007/978-981-99-6641-7_6

The study of spacecraft hovering orbits originated from the exploration of small celestial bodies. Scheeres conducted research on the hovering of spacecraft relative to spinning asteroids [4]. Based on the physical characteristics of small celestial bodies, Broschart and Scheeres defined two concepts of spacecraft hovering small celestial bodies [5]. Lu and Love proposed that the gravitational interaction between Earth and asteroids can enable spacecraft to orbit at a fixed position relative to the asteroid [6].

When the hovering target is a spacecraft, the hovering orbit is divided into circular orbit and elliptical orbit based on different operation orbits. From the perspective of dynamic modeling, Wang et al. [7] deduced the expression of control for the mission spacecraft to achieve hovering at a given position in an elliptical orbit of the target spacecraft. Zhang et al. [8] conducted in-depth research on the impact of different orbit parameters on velocity increment in hovering and explored the hovering feasibility without applying control within certain special parameter variation ranges. In view of the limited fuel carried by spacecraft, a hovering method for electrically charged spacecraft using the hybrid propulsion with conventional chemical propulsion and Lorentz force is proposed [9]. Considering the situation of spacecraft thruster failure, Huang et al. [10] established a dynamic model of underactuated hovering orbit and conducted a detailed analysis of the controllability of the system under underactuated conditions. Furthermore, Huang and Yan [11] proposed an adaptive reduced order observer for speed and parameter estimation in response to disturbance mismatch during underactuated conditions. Huang and Yan [12] designed a backstepping controller to obtain feasible hovering positions under saturated underactuated conditions.

Unlike the previous modeling methods for dealing with J_2 disturbances in spacecraft relative motion, this paper introduces J_2 perturbation as a known term into the hovering orbit dynamics model and obtains the corresponding spacecraft hovering control considering J_2 perturbation. Based on this, the variation law of hovering control under different orbit eccentricity and semimajor axis is obtained. Then, the fuel consumption formula is used to analyze the fuel consumption distribution of different hovering positions for the mission spacecraft in a fixed orbital period, and the selection method for determining the hovering position at the same distance is summarized.

6.2 Hovering Control Considering J_2 Perturbation

In Fig. 6.1, O - XYZ represents ECI (Earth Center Inertia) frame, and M - xyz represents the LVLH (Local Vertical Local Horizontal) frame. In M - xyz , M is the center of LVLH, x is in the radial direction, z is perpendicular to the plane of the target spacecraft's orbit, and y constitutes a Cartesian coordinate system.

The relative dynamics equation is expressed in M - xyz .

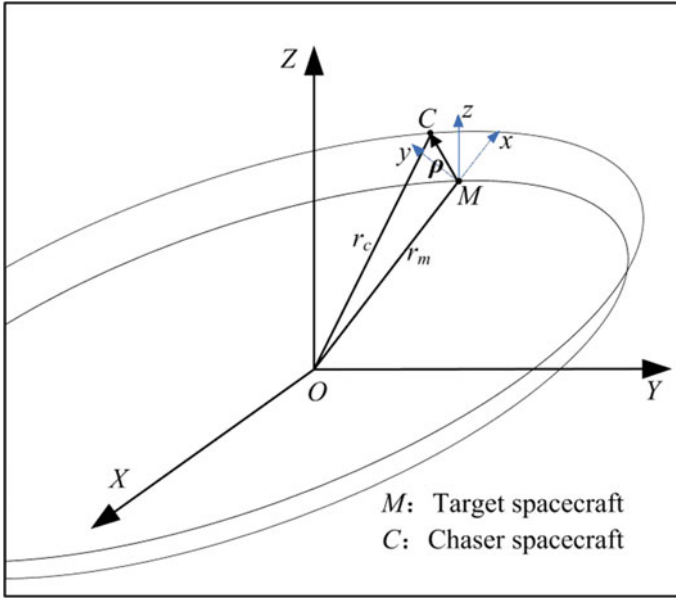


Fig. 6.1 Diagram of relative hovering operation of spacecraft

$$\ddot{\rho} = -2\mathbf{w} \times \dot{\rho} - \mathbf{w} \times (\mathbf{w} \times \rho) - \dot{\mathbf{w}} \times \rho + \frac{\mu}{r_m^3} \mathbf{r}_m - \frac{\mu}{r_c^3} \mathbf{r}_c + \mathbf{f}_c - \mathbf{f}_m + \mathbf{f}_u \quad (6.1)$$

where

- m target spacecraft
- c chaser spacecraft
- μ gravitational constant
- \mathbf{w} orbital angular velocity of the target spacecraft
- $\dot{\mathbf{w}}$ orbital angular acceleration of the target spacecraft
- \mathbf{f}_c external perturbation of the mission spacecraft
- \mathbf{f}_m external perturbation of the target spacecraft
- \mathbf{f}_u control acceleration of the mission spacecraft
- $\rho = [x \ y \ z]^T$ the position vector of the mission spacecraft.

Obviously, Eq. (6.1) is a nonlinear model considering the external perturbation. Based on the relative stationary state characteristics of hovering spacecraft, the state ρ , $\dot{\rho}$ and $\ddot{\rho}$ are as follows:

$$\begin{cases} \rho = \text{const (given)} \\ \dot{\rho} = \ddot{\rho} = \mathbf{0} \end{cases} \quad (6.2)$$

Substituting the relative stationary state characteristics Eq. (6.2) into Eq. (6.1) and taking J_2 gravitational perturbation into account. \mathbf{f}_{uJ_2} is used to denote the required

control acceleration considering J_2 perturbation, and the expression is

$$\mathbf{f}_{uJ_2} = \mathbf{w}_{J_2} \times (\mathbf{w}_{J_2} \times \boldsymbol{\rho}) + \dot{\mathbf{w}}_{J_2} \times \boldsymbol{\rho} + \frac{\mu}{r_{cJ_2}^3} \mathbf{r}_{cJ_2} - \frac{\mu}{r_{mJ_2}^3} \mathbf{r}_{mJ_2} + \mathbf{f}_{mJ_2} - \mathbf{f}_{cJ_2} \quad (6.3)$$

where J_2 denotes the relevant orbital parameters under J_2 perturbation influence. \mathbf{w} and $\dot{\mathbf{w}}$ are given as

$$\begin{cases} \mathbf{w} = [w_{xJ_2} \ w_{yJ_2} \ w_{zJ_2}]^T \\ \dot{\mathbf{w}} = [\dot{w}_{xJ_2} \ \dot{w}_{yJ_2} \ \dot{w}_{zJ_2}]^T \end{cases} \quad (6.4)$$

Merging and simplifying $\mathbf{w}_{J_2} \times (\mathbf{w}_{J_2} \times \boldsymbol{\rho})$ and $\dot{\mathbf{w}}_{J_2} \times \boldsymbol{\rho}$, yields

$$\mathbf{w}_{J_2} \times (\mathbf{w}_{J_2} \times \boldsymbol{\rho}) + \dot{\mathbf{w}}_{J_2} \times \boldsymbol{\rho} = \begin{bmatrix} -w_{zJ_2}^2 & -\dot{w}_{zJ_2} & w_{xJ_2}w_{zJ_2} \\ \dot{w}_{zJ_2} & -w_{xJ_2}^2 - w_{zJ_2}^2 & -\dot{w}_{xJ_2} \\ w_{xJ_2}w_{zJ_2} & \dot{w}_{xJ_2} & -w_{xJ_2}^2 \end{bmatrix} \begin{bmatrix} x \\ y \\ z \end{bmatrix} \quad (6.5)$$

and

$$\mathbf{W}_{J_2} \boldsymbol{\rho} = \mathbf{w}_{J_2} \times (\mathbf{w}_{J_2} \times \boldsymbol{\rho}) + \dot{\mathbf{w}}_{J_2} \times \boldsymbol{\rho} \quad (6.6)$$

\mathbf{S} denotes the transformation matrix (O -XYZ to M -xyz), and the J_2 perturbation of the mission spacecraft in the M -xyz can be converted to

$$\mathbf{f}_{cJ_2} = \mathbf{S} \cdot \mathbf{f}_{cJ_2}^O \quad (6.7)$$

The required control with consideration of the J_2 perturbation can be rewritten as

$$\mathbf{f}_{uJ_2} = \mathbf{W}_{J_2} \boldsymbol{\rho} + \frac{\mu}{r_{cJ_2}^3} \mathbf{r}_{cJ_2} - \frac{\mu}{r_{mJ_2}^3} \mathbf{r}_{mJ_2} + \mathbf{f}_{mJ_2} - \mathbf{S} \cdot \mathbf{f}_{cJ_2}^O \quad (6.8)$$

6.3 Numerical Example

The initial orbital elements of the target spacecraft in the calculation example are shown in Table 6.1.

Table 6.1 Initial orbital elements of the target spacecraft

Orbital element	Value
Semimajor axis (m)	7×10^6
Orbit inclination ($^\circ$)	45
Right ascension of ascending node ($^\circ$)	0
Argument of perigee ($^\circ$)	0
True anomaly ($^\circ$)	0

6.3.1 Variation of Spacecraft Hovering Control Under Different Orbital Elements

Firstly, the influence of eccentricity on the hovering control is analyzed, and the hovering position ρ of the mission spacecraft is set as (1000, 1000, 1000 m). The eccentricity e of the target spacecraft is taken as 0, 0.15, 0.3, 0.45, 0.6, 0.75, and other orbital elements are shown in Table 6.1.

Using Eq. (6.9), the variation of hovering control $|f_{uJ2}|$ in one orbital period with different eccentricity is calculated, as shown in Fig. 6.2.

In Fig. 6.2, when the eccentricity e is 0, the hovering control remains unchanged throughout the orbital period, which means that the corresponding mission spacecraft's hovering orbit is also circular orbit, and its essence is that constant hovering control and earth gravity provide centripetal force to ensure the mission spacecraft's hovering state. When the eccentricity e gradually increases, the hovering control

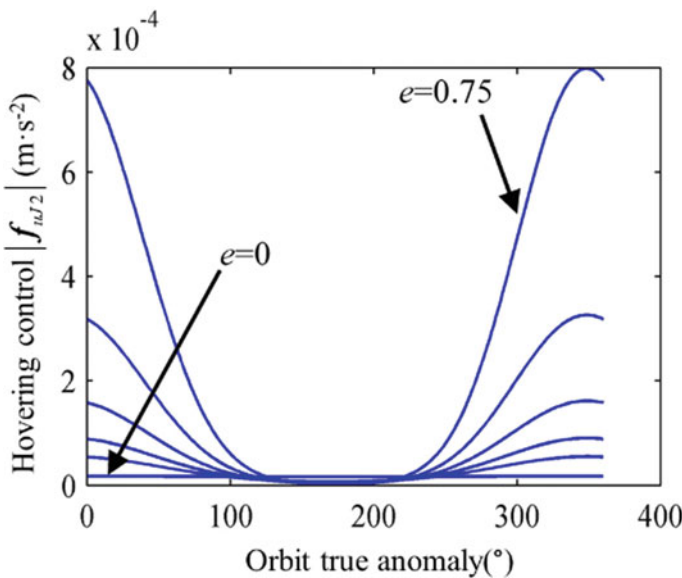


Fig. 6.2 Variation of hovering control with different eccentricity

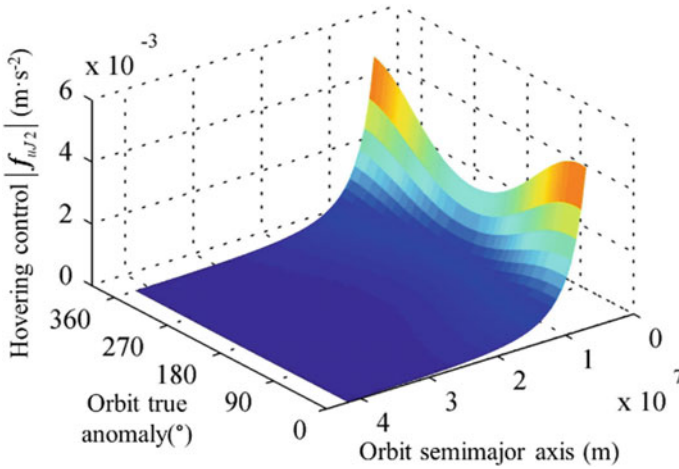


Fig. 6.3 Variation of hovering control with different orbit semimajor axes

near the perigee (when the true perigee is 0°) is large. This is because the semimajor axis a remains unchanged, and the orbital height of the target spacecraft gradually decreases and the angular velocity increases when it approaches the perigee. At this time, the mission spacecraft has to increase the hovering control force to ensure consistency with the orbital angular velocity of the target spacecraft. For the corresponding apogee (when the true near angle is 180°), the required hovering control force is small.

Set the variation range of the semimajor axis a to $7 \times 10^6 \sim 4.2 \times 10^7$ m, the hovering position ρ of the mission spacecraft is also (1000, 1000, 1000) m, the eccentricity is 0.1, and other orbital elements are listed in Table 6.1. The variation of hovering control with different semimajor axes is calculated by using Eq. (6.9), as shown in Fig. 6.3.

From Fig. 6.3, as the semimajor axis a increases, the required hovering control force for the mission spacecraft shows a gradually decreasing trend. When the semimajor axis is 7×10^6 m, the minimum hovering control force in orbital period is $2.6673 \times 10^{-3} \text{ m s}^{-2}$; and the semimajor axis increases to 2×10^7 m, the maximum hovering control force is $2.2882 \times 10^{-4} \text{ m s}^{-2}$, in comparison, the hovering control force decreases by 91.65%. It can be seen that the hovering control force decreases with the increase of semimajor axis throughout the orbital period, and the curve fluctuation of the entire orbital period gradually flattens out. If the hovering distance is constant at this time, the centripetal force of the mission spacecraft in orbit decreases, so the required hovering control force is reduced.

6.3.2 Research on Fuel Consumption in Hovering Orbits

This section mainly analyzes the fuel consumption of the mission spacecraft during the specified mission time. Set the original mass m_0 of the mission spacecraft to 900 kg. In view of the advantage of high specific impulse of electric propulsion, electric thruster is selected to provide continuous control force, and the specific impulse I_{sp} is 29,000 m/s (describe the amount of propellant with mass).

The orbital elements of the target spacecraft are shown in Table 6.1, and the eccentricity e is 0.1. The specified task time is one orbital period, and the range of the true anomaly is $0 \sim 2\pi$, then the fuel consumption formula is as follows Eq. (6.9).

$$\begin{cases} \Delta v = \int_0^{2\pi} |f_{uJ2}| d\theta \\ \Delta m = m_0 \left[1 - \exp\left(-\frac{\Delta v}{I_{sp}}\right) \right] \end{cases} \quad (6.9)$$

where Δv denotes the speed increment, Δm denotes the reduced mass of spacecraft equal to fuel consumption.

Firstly, the fuel consumption of different positions for mission spacecraft hovering is calculated in the x - y plane. The range of values for the hovering positions are $x, y \in [-1000, 1000]$, $z = 0$. Using Eq. (6.9) for calculation, the fuel distribution is given in Fig. 6.4.

From Fig. 6.4a, the fuel consumption gradually increases to 0.7 kg with the increase of x from 0 to 1000 m. As shown in Fig. 6.4b, when $x = 0$ and y ranges from 0 to 1000, the fuel consumption is less than 0.1 kg, indicating that the fuel consumption is less affected by the distance in the y direction. Figure 6.4c further demonstrates that fuel consumption is mainly affected by the position distance in the x direction. Assuming that the hovering distance remains constant at 1000 m, that is, the position distance in the x and y directions meets the condition $\sqrt{x^2 + y^2} = 1000$. The dashed circle in Fig. 6.4c represents the hovering position under assumed conditions, where the specific positions of $A, B, C,$ and D are $(-1000, 0, 0)$ m, $(0, 1000, 0)$ m, $(1000, 0, 0)$ m, and $(0, -1000, 0)$ m, respectively. It is obvious that the fuel consumption at points A and C is the highest. As the hovering position changes with the arrow towards B and D , fuel consumption gradually decreases until it reaches its minimum at points B and D . This indicates that when the mission spacecraft is set in the x - y plane and there are no specific requirements for the hovering position, a larger hovering distance in the y -direction should be selected to reduce fuel consumption.

Similarly, using Eq. (6.9), the distribution of fuel consumption of mission spacecraft is calculated in the y - z plane. The range of values for the hovering position is, $x = 0, y, z \in [-1000, 1000]$ in Fig. 6.5.

Figure 6.5 shows the distribution of fuel consumption in the y - z plane. It is evident that compared to the y direction, the fuel consumption increases faster with the increase of the hovering distance in the z direction. In the y - z plane, the hovering

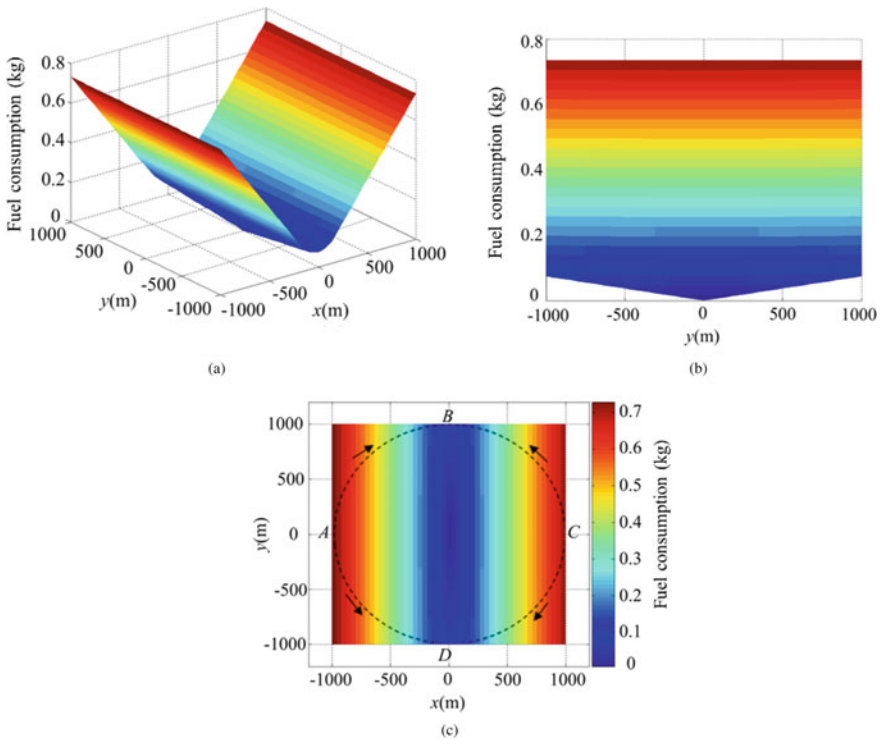


Fig. 6.4 Fuel consumption distribution at different hovering positions in the x - y plane

distance of the y and z directions meets the condition $\sqrt{y^2 + z^2} = 1000$. The dashed circle in Fig. 6.5c represents the hovering position under this condition, where the specific positions of A , B , C , and D are $(0, -1000, 0)$ m, $(0, 0, 1000)$ m, $(0, 1000, 0)$ m, and $(0, -1000, 0)$ m, respectively. Obviously, the fuel consumption at points B and D is the highest. As the hovering position changes with the arrow toward A and C , the fuel consumption gradually decreases until it reaches its minimum at points A and C , indicating that when there are no specific requirements for the specific hovering position, a larger hovering distance in the y direction should be selected to reduce fuel consumption.

Further comparing Figs. 6.4c and 6.5c, it is not difficult to find that under different plane conditions with the same hovering distance, the fuel consumption in the z direction is smaller than that in the x direction. Therefore, the following conclusion is drawn, when the hovering distance is given and the hovering position is uncertain, using reducing fuel consumption as a selection criterion, the first choice is to take a larger distance in the y direction, second in the z direction, and finally in the x direction.

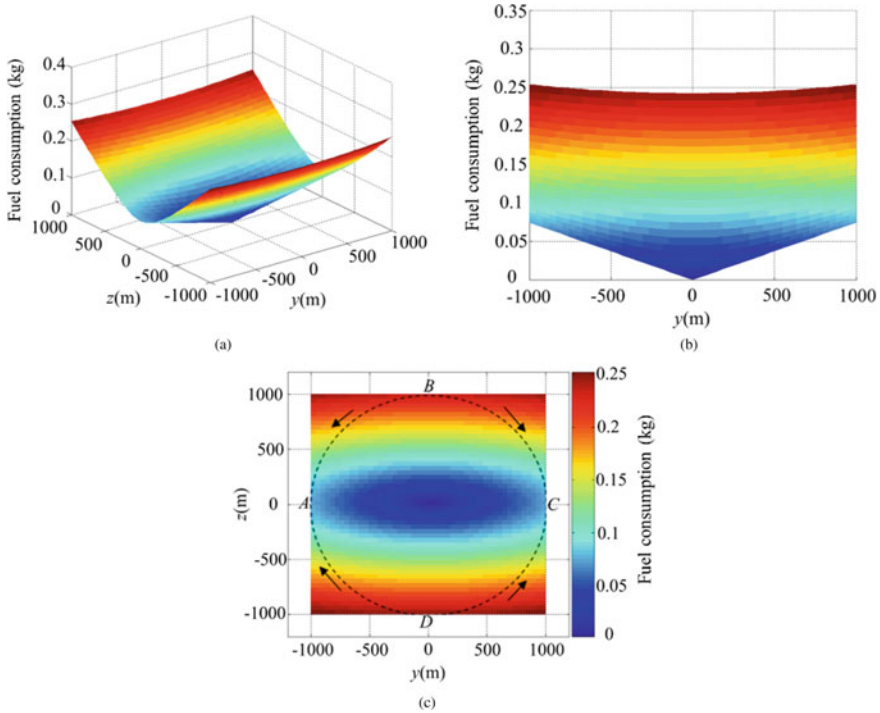


Fig. 6.5 Fuel consumption distribution at different hovering positions in the y - z plane

6.4 Conclusions

This chapter introduces J_2 perturbation into the relative dynamics model of spacecraft and obtains the hovering control equation; the influence of orbit parameters on hovering control is analyzed, mainly focusing on eccentricity and semimajor axis; then the fuel consumption within the determined range is calculated in the x - y plane and y - z plane, and specific fuel distribution cloud maps were provided. The conclusions are as follows:

- (1) When the semimajor axis remains unchanged and the eccentricity e gradually increases, the hovering control near the perigee gradually increases; and the eccentricity e is constant, the hovering control decreases with the increase of semimajor axis throughout the orbit period.
- (2) When the hovering distance of the mission spacecraft is determined, and there is no specific requirements for the hovering position, in order to reduce fuel consumption, the first choice is to take a larger distance in the y direction, second in the z direction, and finally in the x direction.

- (3) Based on the method proposed in this article, the hovering position is selected to achieve the goal of minimizing fuel consumption, prolonging the time of on-orbit service, and providing time guarantee for the successful execution of on-orbit service.

Acknowledgements This study was supported by Ph.D. research startup foundation of University (No. Y-01-2022004) and Tai'an City Science and Technology Innovation Development Project (No. 2022GX042).

References

1. Long, A.M., Richards, M.G., Hastings, D.E.: On-orbit servicing: a new value proposition for satellite design and operation. *AIAA J. Spacecr. Rockets* **44**(4), 964–976 (2007)
2. Ellery, A., Kreisel, J., Sommer, B.: The case for robotic on-orbit servicing of spacecraft: spacecraft reliability is a myth. *Acta Astronaut.* **63**(5), 632–648 (2008)
3. Sellmaier, F., Boge, T., Spurmann, J.: On-orbit servicing missions: challenges and solutions for spacecraft operations. In: *SpaceOps 2010 Conference*, vol. 2159 (2010)
4. Scheeres, D.J.: Stability of hovering orbits around small bodies. In: *AIAA Spaceflight Mechanics Meeting*, 99–159 (1999)
5. Broschart, S., Scheeres, D.J.: Control of hovering spacecraft near small bodies: application to asteroid 25143 Itokawa. *J. Guid. Control Dyn.* **28**(2), 343–354 (2005)
6. Lu, E.T., Love, S.G.: Gravitational tractor for towing asteroids. *Nature* **438**, 177–178 (2005)
7. Wang, G.B., Zheng, W., Meng, Y.H., et al.: Research on hovering control scheme to non-circular orbit. *Sci. China Technol. Sci.* **54**(11), 2974–2980 (2011)
8. Zhang, J., Zhao, S., Yang, Y.: Characteristic analysis for elliptical orbit hovering based on relative dynamics. *IEEE Trans. Aerosp. Electron. Syst.* **49**(4), 2742–2750 (2013)
9. Huang, X., Yan, Y., Zhou, Y., et al.: Sliding mode control for Lorentz-augmented spacecraft hovering around elliptic orbits. *Acta Astronaut.* **103**, 257–268 (2014)
10. Huang, X., Yan, Y., Zhou, Y.: Nonlinear control of underactuated spacecraft hovering. *J. Guid. Control Dyn.* **39**(3), 685–694 (2016)
11. Huang, X., Yan, Y.: Output feedback control of underactuated spacecraft hovering in circular orbit with radial or in-track controller failure. *IEEE Trans. Ind. Electron.* **63**(9), 5569–5581 (2016)
12. Huang, X., Yan, Y.: Saturated backstepping control of underactuated spacecraft hovering for formation flights. *IEEE Trans. Aerosp. Electron. Syst.* **53**(4), 1988–2000 (2017)